1 **Sea ice and pollution-modulated changes in Greenland ice core**

2 **methanesulfonate and bromine**

3 **O.J. Maselli[1*], N.J. Chellman[1], M. Grieman[2], L. Layman[1], J. R. McConnell[1], D. Pasteris[1],**

4 **R.H. Rhodes[3], E. Saltzman[2], M. Sigl[1]**

5 [1] {Desert Research Institute, Department of Hydrologic Sciences, Reno, NV, USA}

6 [2] {University of California Irvine, Department of Earth System Science, Irvine, CA, USA}

7 [3] {University of Cambridge, Department of Earth Sciences, Cambridge, UK}

8 [*] {now at: The University of Adelaide, Australia, 5000}

9 *Correspondence to*:   Olivia Maselli (olivia.maselli@adelaide.edu.au)

11 Keywords: bromine, MSA, nitrate, sea ice, pollution, acidification, Arctic, Greenland, cryosphere

13 **Abstract**

14 Reconstruction of past changes in Arctic sea ice extent may be critical for understanding its future

15 evolution. Methanesulphonate (MSA) and bromine concentrations preserved in ice cores have both

16 been proposed as indicators of past sea ice conditions. In this study, two ice cores from central and NE

17 Greenland were analysed at sub-annual resolution for MSA (CH_3SO_3H) and bromine, covering the time

18 period 1750-2010. We examine correlations between ice core MSA and the HadISST1 ICE sea ice

19 dataset and consult back-trajectories to infer the likely source regions. A strong correlation between the

20 low frequency MSA and bromine records during preindustrial times indicates that both chemical species

21 are likely linked to processes occurring on or near sea ice in the same source regions. The positive

22 correlation between ice core MSA and bromine persists until the mid-20th century, when the acidity of

23 Greenland ice begins to increase markedly due to increased fossil fuel emissions. After that time, MSA

24 levels decrease as a result of declining sea ice extent but bromine levels increase. We consider several

25 possible explanations and ultimately suggest that increased acidity, specifically nitric acid, of snow on

26 sea ice stimulates the release of reactive Br from sea ice, resulting in increased transport and deposition

27 on the Greenland ice sheet.

1 Introduction

30 Atmospheric chemistry in the polar regions is strongly modulated by physical, chemical, and biological

31 processes occurring in and around sea ice. These include sea salt aerosol generation, biogenic emissions

32 of sulphur-containing gases and halogenated organics, and the photochemical/heterogeneous reactions

33 leading to release of volatile, reactive bromine species. The resulting chemical signals influence the

34 chemistry of the aerosol deposited on polar ice sheets. For this reason ice core measurements of sea salt

35 ions, methanesulphonate (MSA), and bromine have been examined as potential tracers for sea ice extent

36 (Abram et al., 2013; Spolaor et al., 2013b, 2016; Wolff et al., 2003). The interpretation of such tracers

37 is complicated by the fact that their source functions reflect changes in highly complex systems, and

38 signals are further modified by patterns of atmospheric transport and deposition.

39 MSA is produced by the atmospheric oxidation of DMS ($(CH_3)_2S$). DMS is produced throughout the

40 world's oceans as a breakdown product of the algal metabolite DMSP, ($(CH_3)_2S^+CH_2CH_2COO^-$).

41 DMS emissions are particularly strong in marginal sea ice zones (Sharma et al., 2012), and this source

42 is believed to be a dominant contributor to the MSA signal in polar ice (Curran and Jones, 2000). Ice

43 core MSA records have been used extensively in Antarctica as a proxy for local sea ice dynamics.

44 Although the specifics of the relationship are highly site-dependent (Abram et al., 2013; Curran et al.,

45 2003) MSA has been proven to be a reasonably good proxy for sea ice conditions (e.g., (Curran and

46 Jones, 2000)). In the Arctic, the relationship between MSA and sea ice conditions is less straightforward

47 due to the likelihood of multiple source regions with different sea ice conditions contributing to the ice

48 core archived MSA (Abram et al., 2013). Until now, a significant, but rather weak (r =-0.37)

49 relationship between ice core MSA and Arctic sea ice has only been established for a record from a

50 Svalbard ice core (O'Dwyer et al., 2000). In this study we analyse the direct correlations between the

51 MSA records from two Greenland ice core sites and the surrounding sea ice conditions in order to

52 demonstrate the utility of MSA as a local sea ice proxy.

53 In this study, all dissolved or suspended bromine species are measured (including organic bromine) and

54 shall be referred to as "bromine". The primary source of total inorganic bromine (e.g. Br_2, Br^-, HBr)

55   in the marine boundary layer (MBL) is the ocean (Parrella et al., 2012; Sander et al., 2003). At

56 concentrations of less than 0.2% that of sodium (Na), bromide (Br^-) makes a small contribution to

57 ocean salinity. Br^- can be concentrated in the high latitude oceans when the sea water is frozen, since

58 the formation of the ice matrix exudes the sea-salts in the form of brine (Abbatt et al., 2012). Small, sea-

59 salt aerosol particles blown from the surface of sea ice are typically enriched with bromine (Sander et

60 al., 2003) and satellite imagery has revealed that plumes of bromine (as BrO) are photo-chemically

61 released from sea-ice zones in spring (Nghiem et al., 2012; Schönhardt et al., 2012; Wagner et al., 2001).

62 Recently, studies have begun to link ice core records of bromide enrichment (relative to sea water Na

63 concentrations) preserved in polar ice sheets to that of local sea ice conditions (Spolaor et al., 2013a,

64 2013b, 2014). Spolaor and co-workers demonstrated the spring-time Br^-/Na that is preserved in the

65 ice core is a record of bromine explosion events over adjacent seasonal sea ice. A Br^-/Na enrichment

66 would therefore indicate a larger seasonal sea ice extent or conversely a shorter distance between the

67 ice edge and the ice core site due to decreased multi-year sea ice (Spolaor et al., 2013a). However, like

68 MSA, it is likely that the bromine – sea-ice relationship in the Arctic is complicated by the myriad of

69 bromine source regions which influence an ice core record in addition to factors which influence the

70 degree of enrichment of the aerosol as it travels to the ice core site. In this study we compare ice core

71 records of bromine to those of MSA and other common MBL species in order to determine the influence

72 of sea ice conditions and other factors on bromine concentrations.

73 Here we present measurements of MSA, bromine, and elemental tracers of sea salt and crustal input in

74 two Greenland ice cores covering the time period 1750-2010 C.E.. These ice core records represent the

75 first continuous, sub-annual resolution records of bromine in polar ice to extend beyond the satellite era.

76 We examine the relationship between these two sea ice-modulated tracers, their relationship to

77 independent historical estimates of sea ice distribution, and the influence of industrialization on

78 atmospheric and ice core chemistry.

79 **2   Methods**

80 **2.1   Ice cores**

81 The 87 m 'Summit-2010' ice core was collected in 2010 close to Summit Station, Greenland (72°20'N

82 38°17'24"W). The average snow accumulation at Summit is ~0.22 m yr^{-1} water equivalent, with few

83 instances of melt. Due to the relatively high snow accumulation rate, seasonal analysis of the sea salt

84 species concentrations was feasible. The 213 m Tunu core was collected in 2013 (78° 2' 5.5"N, 33° 52'

85 48"W), approximately 3 km east of the Tunu-N automatic weather station, part of the Greenland Climate

86 Network. The average snow accumulation at Tunu is ~0.11 m yr^{-1} water equivalent. The Summit-2010

87 and Tunu cores were dated using well-known volcanic horizons in sulfur (S). The dating of Summit-

88 2010 was refined by annual layer counting using seasonal cycles in the ratio of non-sea salt S/Na (Sigl

89 et al., 2015).

2.2 Sampling and analysis

The ice cores were sampled from 33x33 mm cross-section sticks using a continuous melter system (McConnell et al., 2002). The silicon carbide melter plate provides three streams from concentric square regions of the ice core sample: an innermost stream (with a cross sectional area of 144 mm^2), an intermediate stream (340 mm^2) and an outer stream that was discarded along with any contaminants obtained from handling of the ice core. The innermost melt stream was directed to two inductively coupled plasma-mass spectrometers (ICP-MS, Thermo Element II high resolution with PFA-ST concentric Teflon nebulizer (ESI)) run in parallel. All calibrations and runtime standards were run on both instruments and several elements were also measured in duplicate (Na, Ce, Pb) to ensure tracking between both ICP-MS. In addition, an internal standard of yttrium flowed through the entire analytical system and was used to observe any change in system sensitivity. The instrument measuring bromine was run at low resolution to get the highest sensitivity and there were no mass interferences observed at the bromine isotope mass monitored (79 amu). The sample stream was acidified to 1% HNO_3 to prevent loss of less soluble species, degassed just prior to analysis to minimize mixing in the sample line and sampled at a rate of 0.45ml min^{-1} (McConnell et al., 2002; Sigl et al., 2013). The following elements were measured by ICP-MS: Br, Cl, Na, Ca, S, Ce, and Pb. Calibration of the ICP-MS was based on a series of 7 mixed standards measured at the start and end of each day for all elements except for the halides. Due to the high volatility of acid halides, a set of 4 bromine and chlorine standards were made individually in a 1% UHP HNO_3 matrix from fresh, non-acidified intermediate stock solution (Inorganic Ventures) every day. The intermediate melt stream was directed to a continuous flow analysis (CFA) system on which nitrate ion (NO_3^-) and snow acidity (sum of soluble acidic species) were measured using the technique described by Pasteris (2012) in addition to other atmospheric species of interest (Röthlisberger et al., 2000).

A portion of the debubbled CFA melt stream (150 µl min^{-1}) was subsampled using a peristaltic pump for continuous on-line analysis of methanesulfonate by electrospray triple-quad mass spectrometer (ESI/MS/MS; Thermo-Finnigan Quantum). This subsample was mixed with pure methanol (50 µl min^{-1}) delivered using an M6 pump (VICI). The methanol was spiked with an internal standard of deuterated MSA ($CD_3SO_3^-$; Cambridge Isotopes) at a concentration of 52 nM. The isotope standard was calibrated against non-deuterated MSA standards prepared in water from non-deuterated MSA ($CH_3SO_3^-$; Sigma Aldrich). MSA was detected in negative ion mode using the $CH_3SO_3^-/SO_3^-$ transition (m/z 95/80) and $CD_3SO_3^-/SO_3^-$ (m/z 98/80). The concentration of MSA in the sample flow was determined from the ratio of the non-deuterated and deuterated signals after minor blank corrections. The analysis of MSA by batch analysis using ESI/MS/MS has been reported previously (Saltzman et al., 2006). This study is

123 the first use of the technique for ice core MSA analysis in a continuous, on-line mode. The uncertainty

124 in the MSA intensity as calculated from the standard calibrations is 1%.

2.3 Calculation of anthropogenic Pb, non sea-salt S, and Br enrichment

126 The Pb derived from anthropogenic sources (exPb) was calculated as the difference between total lead

127 and that from dust sources:

$$\mathbf{exPb} = [\mathbf{Pb}]_{\mathbf{obs}} - [\mathbf{Ce}]_{obs} \times \left(\frac{[\mathbf{Pb}]}{[\mathbf{Ce}]}\right)_{\mathbf{dust}}$$

(1)

130 Where the $([Pb]/[Ce])_{dust}$ mass ratio has the constant value of 0.20588 (Bowen, 1979).

131 Similarly the amount of non-sea salt sulphur (nssS) was calculated relative to the sea-salt sodium, ssNa:

$$\mathbf{nssS} = [\mathbf{S}]_{\mathbf{obs}} - [\mathbf{ssNa}] \times \left(\frac{[\mathbf{SO_4^{2-}}]}{[\mathbf{Na}]}\right)_{\mathbf{seawater}}$$

(2)

133 Where the $\left(\frac{[SO_4^{2-}]}{[Na]}\right)_{seawater}$ mass ratio has the constant value of 0.252 (Millero, 1974). ssNa was

134 calculated by comparison with calcium as both have sea salt and dust origins (Röthlisberger et al., 2002):

$$\mathbf{ssNa} = \frac{[\mathbf{Na}_{\mathbf{obs}} \times \mathbf{R}_{\mathbf{t}} - \mathbf{Ca}_{\mathbf{obs}}]}{[\mathbf{R}_{\mathbf{t}} - \mathbf{R}_{\mathbf{m}}]}$$

(3)

139 Where R_t and R_m are the Ca/Na mean crustal and mean marine mass ratios of 1.78 and 0.038,

140 respectively, (Millero, 1974).

141 Bromine enrichment factors relative to sea water concentrations were calculated using the following:

$$\mathbf{Br}_{\mathbf{enrich}} = \left(\frac{[\mathbf{Br}]}{[\mathbf{Na}]}\right)_{\mathbf{obs}} \bigg/ \left(\frac{[\mathbf{Br}]}{[\mathbf{Na}]}\right)_{\mathbf{seawater}}$$

(4)

144 where the $([Br]/[Na])_{seawater}$ mass ratio is 0.00623 (Millero, 1974).

2.4 Air mass- back trajectories

146 To identify the likely sea ice source regions of MSA and Br deposited at the ice core sites, we perform

147 10 day air-mass back trajectories of boundary layer air masses from each ice core site using the GDAS1

148 archive dataset in the Hysplit4 software (Draxler and Hess, 1998). The starting height of the back

149 trajectories was 500 m to ensure that the monitored air masses travelled close enough to the surface at

150 the ice core site to potentially deposit aerosols. The vertical velocity field was taken from the

151 meteorological data files. Air mass back trajectories were started every 12 hours and allowed to travel

152 for 10 days (total number of trajectories hours = 14400 hours per month). The number of hours that the

153 trajectories spent in a 2°x2° degree grid was summed over all of the trajectories for that month between

154 the years 2005-2013. Previous work showed that the rapid advection of MBL air was the likely source

155 of reactive halogens at Summit (Sjostedt et al., 2007).

2.5 Sea Ice Correlation mapping

157 In order to assess the relationships between sea ice conditions and ice core chemistry, correlation maps

158 were generated between annual MSA concentrations and monthly sea ice using the HadISST1 ICE

159 dataset at 1° latitude-longitude monthly resolution (Rayner, 2003). Pre-1979 sea ice datasets were

160 interpolated from sea ice extent maps compiled by Walsh (1978) which incorporate a variety of

161 empirical observations. The data were later bias corrected using modern satellite data (Rayner, 2003).

162 Correlations were performed separately for the satellite period (1979-2012) and for the extended record

163 (1900-2012), excluding the period 1940-1952 when the record has no variability due to scarcity of data

164 (Rayner, 2003). Because strong DMS emissions occur in marginal sea ice zones (Sharma et al., 2012),

165 we considered both sea ice concentration (SIC) and the area of open water in the sea ice pack (OWIP)

166 which represents the size of the marginal sea ice zone. OWIP is defined as the difference between sea

167 ice area (calculated from sea ice concentration over the area of the grid cell) and sea ice extent (NSIDC).

168 A SIC of 15% was used as the threshold for a grid cell to contribute to sea ice extent. The area of OWIP

169 was calculated within the coastal areas as defined by the results of the air-mass back trajectories (Sect.

170 3.4).

171 Correlations were performed on an annual rather than seasonal basis because the seasonality of ice core

172 MSA is distorted due to post depositional migration of MSA signal at depth in the snow pack (Mulvaney

173 et al., 1992) (Fig. 3, S3). Outliers were removed from the MSA time series (see Fig. 2) before the

174 correlations were performed using the technique described by Sigl (2013) for identifying volcanic

175 signals using a 25 year running average filter.

176

3   Results

3.1   Bromine

Ice core measurements of bromine at Summit and Tunu covering the period 1750-2010 are shown in Fig. 2. Ice core Br levels at each site were stable until ~1830 when they decreased by ~1 nM, establishing a new baseline that was stable until the early 1900s. Both ice cores also show a Br peak in the late 20th century. A summary of the timing of inflections and concentrations can be found Table S1.

Sea-salt transport onto the Greenland ice sheet occurs predominantly during winter. Historically the winter-time sea-salt maximum was believed to be due to increased cyclonic activity over the open oceans (Fischer and Wagenbach, 1996) though more contemporary studies show that blowing snow from the surface of sea-ice may be a significant source (Rankin et al., 2002; Xu et al., 2013; Yang et al., 2008, 2010). At Summit, a winter-time maximum is observed in the most abundant sea salts, Na and Cl (Fig. 3). Bromine also shows a significant winter-time signal, however the annual maximum appears in mid-summer - at concentrations ~70% above winter levels (Fig. 3a). Comparison with Br measured in weekly surface snow samples collected from Summit (from 2007-2013; GEOSummit project) confirms that this summer signal is real and not a result of post-depositional modification of seasonality of the bromine signal (Fig. S1). The results from that study confirm that total Br concentrations peak in summer on the ice sheet closely following the Br cycle observed in the Summit-2010 ice core. In addition to the comparison with the Geosummmit data, in the ice cores studied here there are routinely more than 10 measurements made within a yearly layer of snow giving confidence to the allocation of a summer maximum in bromine at Summit. Analysis of the annual cycle of bromine in the Tunu ice core also shows a summer maximum when averaged over the entire ice core time series but with significantly larger error than observed at Summit. The timing of this peak suggests a predominant summer source of bromine that dwarfs that from winter sea salt sources.

The shape of the annual bromine cycle does change slightly over the course of the Summit record (see Fig. 3). Starting in the early 1900s the annual bromine cycle slowly becomes broader. A slight shift in the maximum from a solely summer peak in the preindustrial era towards a broad summer-spring peak by 1970 is observed (Fig. 3 lower plot). Comparison with the sea salt tracer, sodium, which does not undergo the large temporal shift and broadening of its seasonal cycle shows that this change in bromine seasonality is not linked to changes in production or transport of sea-salt aerosols or even dating uncertainties in the ice core but perhaps the introduction of an additional, smaller bromine source in the spring-time during the industrial era.

Both ice cores show a predominantly positive Br enrichment throughout the year (Fig S2) relative to

209 both sea salt elements chlorine and sodium. This enrichment reaches a maximum in mid to late summer

210 at Summit (Fig 3). We assume that this enrichment reflects Br enrichment in the aerosol transporting

211 Br to the ice sheet. However, post-depositional reduction of the bromine concentration is a possibility

212 during the summer months due to photolytic processes at the snow surface. This may be the cause of

213 the noisiness of the bromine signal within the lower accumulation, Tunu core. However, the increased

214 snow accumulation that occurs during the summer months in both central and northern Greenland (Chen

215 et al., 1997) should act minimise these bromine depleting effects driven by increased insolation in

216 summer.

217 A summer time maximum in Br enrichment was also observed by Spolaor (2014) in a short segments

218 of Antarctic Law Dome ice core as well as two Arctic ice cores. Spolaor et al. believe that the main

219 source of the inorganic bromine originated from spring-time bromine explosion events above sea ice

220 and the summertime maximum could possibly be an indication of lag-time between bromine containing

221 particles becoming airborne and their deposition. Further investigation is needed to definitively establish

222 the seasonality of bromine deposition at the poles. However the results of the Arctic ice cores studied

223 here suggest that the summer maximum in bromine deposition is indeed real.

224 In the Tunu ice core, 2% of the monthly bromine enrichment measurements (relative to Cl) were

225 negative (less than the Br/Cl seawater ratio, Fig S2). In a comprehensive review of global aerosol Br

226 measurements, Sander (2003) concluded that in general, aerosols which showed positive Br enrichment

227 factors were of sub-micrometer size. These small aerosols can travel further (lifetimes of around 5-10

228 days) and due to their larger surface/volume ratio may experience more atmospheric processing than

229 larger aerosols, resulting in the positive enrichment. It is possible that the negative enrichment values

230 observed in the Tunu ice core are therefore a result of larger aerosols (> micrometer) reaching the site

231 due to its proximity to the coast (and thus the likely sea ice aerosol source region) in comparison to

232 Summit.

3.2 MSA

234 The Summit-2010 MSA record (Fig. 2) replicates that measured by Legrand in 1993 (Legrand et al.,

235 1997) and extends it an additional 17 years. The Tunu measurements represent the first MSA profile at

236 this location. At Summit, MSA concentrations averaged 48 nM in the late 18th century, compared with

237 just 27 nM at Tunu. From 1878-1930 MSA concentrations at Summit plateaued at 36 nM after which

238 they began to   drop rapidly, at a rate of 0.27 nM/year, reaching 18 nM by 2000. Large fluctuations in

239 the MSA record after this time make it difficult to assess the most recent trend in Summit MSA

240 concentrations. MSA concentrations in the Tunu core showed a similar variability to those in the

241   Summit record, and until the mid-20th century, were consistently lower in magnitude. MSA

242   concentrations only began to decline consistently at Tunu after 1984, almost 50 years after the rapid

243   decline observed in the Summit record. After 2000, large fluctuations in concentration were again

244   observed making the modern-day trend in MSA concentration at Tunu difficult to establish.

245   Comparison with the total sulfur record (Fig. 4) reveals that during the preindustrial period, MSA

246   contributes to ~12% and ~ 7% of the total sulfur signal at Summit and Tunu, respectively, compared

247   with < 2% at the height of industrial period (1970 C.E.) at both sites.

248   The low frequency, preindustrial trend in MSA concentrations seen in these ice core records closely

249   follows that of bromine; particularly distinct is the decrease in both MSA and bromine at both sites in

250   the early 1800s (Tables S1and S2). In the early 1900s, however, both sites show a divergence between

251   the MSA and Br records—as MSA begins to decline, Br concentrations increase.

252   A dramatic shift in the 'timing' of the annual MSA maximum in Summit-2010 ice core is illustrated in

253   Figs. 3c and S3. The signal shifts gradually and continuously along the length of the the entire Summit-

254   2010 record from a spring to winter maximum (Fig. S3). This phenomenon has previously been

255   observed in several Antarctic ice cores and has been attributed to post-depositional migration within the

256   ice due to salt gradients (Mulvaney et al., 1992; Weller, 2004).

3.3 Acidic Species

258   In winter, with the collapse of the polar vortex, polluted air masses enter the Arctic region as the

259   phenomenon known as the Arctic haze (Barrie et al., 1981; Li and Barrie, 1993). SO_2 and NO_x from the

260   haze are deposited on the ice/snow and oxidised to sulphuric (H_2SO_4) and nitric acid (HNO_3). There are

261   also natural sources of SO_2 (biomass burning, volcanic eruptions, oceans (Li and Barrie, 1993;

262   McConnell et al., 2007; Sigl et al., 2013) and NO_x(microbial activity in soils, biomass burning, lightning

263   discharges (Vestreng et al., 2009) as well as other snow/ice acidifiers including MSA, hydrogen chloride

264   and organic acids released from biogenic or biomass burning sources (Pasteris et al., 2012).

265   Total snow acidity was stable at both sites from 1750 through to ~1900 except for sporadic, short-lived

266   spikes due to volcanic eruptions. The average preindustrial acidity was the same at both sites (~1.8 μM).

267   Both records also show two distinct maxima in acidity centred on 1920 and 1970 (Fig. 4) with Tunu

268   displaying higher acidity than Summit over the entire industrial period. Overlaid with the acidity is the

269   total sulphur (S) record for both ice cores. The high correlation between the acidity and S records

270   illustrates that the sulphur species are the dominant natural and anthropogenic acidic species in the ice

271   cores. The trend in acidity closely follows the global SO_2 emissions with maxima from coal (~1920)

272   and fossil fuel combustion (~1970), respectively (Smith et al., 2011). After 1970 the records of acidity

273   and S deviate. This deviation can be attributed to the presence of nitric acid that remains at a relatively

274   high concentration in the late 20th century whilst sulphur species reduce in concentration (Fig. 4).

275   NO_3^- concentrations show no trend during the preindustrial era in either ice core records, averaging

276   1.1(±0.02) µM and 1.3(±0.03) µM for Summit and Tunu, respectively. The higher signal-to-noise ratio

277   in the Summit-2010 record reveals a small peak in NO_3^- concentrations centred on ~1910. The Tunu

278   record also shows elevated NO_3^- concentrations over this period. However the large variability in the

279   signal makes it difficult to establish a higher resolution temporal trend. Both records clearly show a

280   large increase in NO_3^- after 1950, peaking in ~1990 and followed by a general decreasing trend with the

281   average until 2010 C.E. NO_3^- levels still double that of preindustrial concentrations: 2.1µM and 2.3 µM

282   at Summit and Tunu, respectively.

283   The nitrate records from both sites follow the trend in northern hemisphere NO_x emissions with a peak

284   in ~1910 and 1990 C.E.– a result of emissions from increases in both Northern Hemisphere fertilizer

285   usage and biomass and fossil fuel combustion (Felix and Elliott, 2013).

3.4   Air mass back trajectories

287   Air mass back trajectory results demonstrate that air masses reaching the Summit-2010 site between

288   March and July originate primarily from the South/South-East of the ice core site (Fig. 5a). Previous

289   back trajectory analyses by Kahl *et al*. (1997) also linked individual spikes in their Summit MSA record

290   to air masses that had passed over this same region of coast (SE Greenland) within the previous 1-3

291   days.Similar back trajectories were calculated for Summit-2010 at heights of 500 and 10,000m (Fig. 5a,

292   S4a) illustrating that air masses that travel in the free troposphere and lower troposphere follow similar

293   back trajectories and likely share the same source regions.

294   The results for Tunu indicate that air masses arrive primarily from the west coast of Greenland, passing

295   over the Baffin Bay area, but there is also significant contribution from both the SE and NE (in May)

296   coastal areas (Fig. 6b, S4b). Of these two secondary areas it is likely that aerosols transported from the

297   NE would have a greater influence on the ice core concentrations due to proximity to the ice core site.

298   Aerosol deposited at Tunu therefore represents a mixture of source regions, but are likely dominated by

299   the NW Greenland, Baffin Bay coastal region.

3.5   MSA - Sea Ice correlations

301   Locations which showed a sea ice concentration (SIC) variability greater than 10% (the average

302   estimated range of uncertainty in the satellite measurements) and have a significant correlation to MSA

303   (t-test, $p<0.05$) are displayed in Fig. 6 and 7. A greater weight must be placed on the post-1979 sea ice

304   concentration maps (Fig. 6b, Fig. 7b) as these were derived from passive microwave satellite data and,

305   where available, operational ice chart data. The likely air-mass source regions, as defined by the results

306   of the air-mass back trajectories, are indicated by the black bordered regions in Figs. 6 and 7. Within

307   these areas there is generally a negative correlation between SIC and MSA, particularly in the spring

308   months. The large areas of positive correlation along the east coast and in the western Barents Sea are

309   striking, however, these areas are outside of the defined air-mass source region and thus are unlikely to

310   be contributing to the ice core aerosol records. The positive correlation is likely an artefact of the

311   negative autocorrelation between sea ice conditions in this region and the SE coast source region (Fig.

312   S5).

313   Over the period 1900-2010 C.E. highly significant correlation (t-test, $p<0.001$) is found between the

314   annual ice core MSA and the amount of open water in the ice pack (OWIP, representing the area of the

315   marginal sea ice zone, Fig. 6a, Fig. 7a) in these aerosol source areas. For both ice cores the source region

316   OWIP is stable until ~1970, when it begins to decline; a trend followed by the MSA. Over the shorter,

317   satellite era (1979–2010), both the Summit-2010 and Tunu sites show strongest correlation between

318   annual MSA and OWIP in March – when the break-up of the winter sea ice begins ($r = 0.33$, $p< 0.1$; r

319    $= 0.37$, $p<0.05$, Fig. 7b, Fig. 8b). The significance of the Tunu correlation over this period can be

320   dramatically increased ($r = 0.58$; $p<0.001$), if the closer, secondary source region (NE Greenland) is

321   assumed to also influence the site (not shown).

3.6   MSA and bromine relationship

323   In an era where climate is driven by only natural forcings, chemical species that share a common source

324   should show broadly consistent variability. This is evident in the preindustrial section of both ice core

325   records where the relationship between MSA and Br (monitored as Br/MSA) remains constant over the

326   entire period (Fig. 4) despite individual records going through step function changes. Using a 25 year

327   running average on all records, the correlation between MSA and Br over the preindustrial period was

328   calculated as: Summit-2010: r=0.282 (p=0.0008); Tunu: r= 0.298 (p = 0.0004), n= 138. After ~1930,

329   relative increases in Br concentrations cause the Br/MSA ratio to increase above the stable preindustrial

330   levels by more than 160%, reaching a peak in ~2000 C.E. at both sites.

331   Bromine in excess of what is expected from a purely sea ice source (exBr) was calculated by comparison

332   to the other sea ice proxy, MSA. A linear regression of Br versus MSA was performed with the

333   preindustrial data to establish the relationship between the two proxies during an era free of

334   anthropogenic forcing. This relationship was then extrapolated into the period after 1850 C.E. in order

335   to estimate the amount of bromine sourced only from sea-ice sources during the industrial era. The MSA

336 record was smoothed with a 264 point Stineman function before being used in the extrapolation to

337 reduce the noise in the resultant record whilst maintaining the low frequency trends. exBr is thus the

338 difference between the total bromine measured and the calculated, natural sea ice bromine (in contrast

339 to Br_{exc} defined by Spolaor (2016) as the amount of bromine in excess of the Br/Na seawater ratio).

340 An estimate of the amount of bromine measured in excess of what is expected from a purely sea ice

341 source (exBr) is shown is Fig. 8. By definition, exBr is constant during the preindustrial period, but

342 during the industrial period exBr peaks, reaching a broad maximum between 1980-2000 C.E. of ~2nM

343 and 5nM at Summit and Tunu, respectively.

4   Discussion

345 The significant correlation between variability of marginal sea ice zone (OWIP) area within the

346 identified source regions and the MSA records suggests that MSA records can be used as a proxy for

347 modern sea ice conditions in these areas. Assuming that no major changes in atmospheric circulation

348 patterns occurred to change the source regions for the marine aerosols between the preindustrial and

349 industrial periods, our identification of MSA as a sea ice proxy (specifically a marginal sea ice zone

350 proxy) may be valid for time periods both before and after 1850 at each ice core site. One major Northern

351 Hemisphere climate phenomena is the North Atlantic Oscillation (NAO).   NAO proxy records

352 developed in Greenland ice core records (Appenzeller et al., 1998) suggest that although the NAO has

353 shown variability over the past 200 years, its effect is damped in Northern Greenland (Appenzeller et

354 al., 1998; Weißbach et al., 2015).

355 The MSA records reveal that after 1820 a gradual decline in sea ice occurred along the southern

356 Greenland coast (reflected in the Summit-2010 core) and that this decline in sea ice did not extend

357 significantly to the most northern Greenland coastline (reflected in the minimal change in Tunu MSA

358 during this period). It is not unexpected that the Summit-2010 record would show the most dramatic

359 changes in sea ice since we have demonstrated that the Summit sea ice proxy (MSA) is sourced from

360 the south-east Greenland coast – an area sensitive to climate changes as it is primarily covered by young,

361 fragile sea ice. The timing of the sea ice decline is coincident with the end of the Little Ice Age, identified

362 from $\delta^{18}O$ ice core records as spanning the period 1420-1850 A.D. in Greenland (Weißbach et al., 2015).

363 The dramatic dip in sea ice reflected in both the Tunu MSA and Br records at 1830 A.D. (and also seen

364 less dramatically in Summit) also appears in the multi-proxy reconstruction of sea ice extent in the

365 Western Nordic Seas performed by Macias Fauria et. al. (2010). This may be evidence of a sea ice

366 decline event isolated to the east Greenland coast as the ice core records do not replicate the dramatic,

367 early 20th century fluctuations observed in the latter part of the Western Nordic Seas reconstruction.

368 From the ice core records it appears that the greatest decline in Greenland sea ice began in the mid 20th

369 century, dropping to levels that are unprecedented in the last 200 years. This decline is observed along

370 the entirety of the Greenland coast. Sea ice declined first around the southern coast (from 1930 A.D.,

371 reflected in Summit-2010) followed 54 years later by the more northern coastline (reflected in the Tunu

372 record, see infection timings in Table S1). This sea ice decline is coincident with the sustained increase

373 in greenhouse gases which has been identified as the major climate forcing and driver of increased

374 global temperatures during the 20th century (Mann et al., 1998) and follows the same general trend in

375 Arctic wide sea ice extent observed by Kinnard (2008).

376 Bromine has also been suggested as a possible proxy for sea ice conditions, however the timing of the

377 largest bromine aerosol flux, in summer, does not coincide with the largest growth or extent of new sea

378 ice. Sea ice begins to increase only at the end of summer as the fractures in the ice cover are re-laminated

379 and the ice edge begins to advance southward (see Fig. 3f).

380 So what is the summer-time source of bromine? What is the cause of the increase in spring-time bromine

381 explosion events in the industrial era? (see Fig. 3, lower panel) and why does the bromine record deviate

382 from the sea ice proxy record (MSA) around the same time? Possible sources of bromine and the factors

383 which may effect the resultant bromine flux are discussed below.

4.1 Alternate sources of bromine

4.1.1 Combustion of coal

386 Bromine is present in coal (Bowen, 1979; Sturges and Harrison, 1986) and coal burning is therefore a

387 potential source of increased bromine deposition on the Greenland ice sheet over the period 1860-1940

388 (McConnell and Edwards, 2008). McConnell et al. (2008; 2007) demonstrated that pollution from the

389 Northern American coal burning era was deposited all over Greenland leaving as its fingerprint large

390 amounts of black carbon and toxic heavy metals. Sturges (1986) measured the relative concentrations

391 of Br and Pb in particulates emitted from the stacks of coal fired power stations and found a molar ratio

392 (Br:Pb) ranging between 0.36-0.67:1. Figure 8 illustrates that at both Summit and Tunu the exPb (lead

393 not from dust sources) preserved in the ice cores over the coal burning era was less than 1nM. This

394 concentration implies that the upper limit to the amount of bromine deposited from coal combustion

395 would be 0.67nM (assuming no loss of bromine from the particulates during transportation). This is an

396 insignificant amount compared to the total Br signal preserved in the ice at this time. Coal combustion

397 is not the major cause of the elevated industrial Br concentration.

4.1.2 Leaded Gasoline

398
399 The largest historical, anthropogenic source of bromine is thought to be the combustion of leaded
400 gasoline. Large quantities of 1,2, diethyl bromide (DEB) were added to leaded fuel as a scavenger for
401 Pb preventing lead oxide deposition by converting it to volatile lead bromide salts as well as CH_3Br
402 (Oudijk, 2010;Nriagu, 1990;Berg et al., 1983). In 1925 gasoline had a Br:Pb molar ratio of 2:1 in a
403 formulation which is now called "aviation fluid'. The Br:Pb molar ratio was reduced to 1:1 in the 1940s
404 except in places such as the Soviet Union which continued to use "aviation fluid" for motor gasoline
405 (Thomas et al., 1997). Although the consumption of leaded gasoline has been well documented,
406 particularly in North America, the estimates of the emissions of bromine compounds from the
407 combustion process are still unclear. Estimates of the amount of DEB that is converted into gaseous
408 CH_3Br range from 0.1% to 25% (Bertram and Kolowich, 2000) and direct measurements of exhaust
409 fumes across NW England found a Br:Pb ratio of between (0.65-0.8):1 in the airborne particulates
410 (Sturges and Harrison, 1986).

411 The ratio of Br:Pb in the gasoline formulae can therefore be used only as an upper limit to predict the
412 Br:Pb ratio in gasoline combustion aerosols transported to the ice core sites. Figure 8 shows a
413 comparison between exBr and exPb measured in each ice core. Also illustrated is the upper limit of the
414 amount of bromine expected from gasoline sources assuming the 2:1 Br:Pb ratio for aviation gasoline
415 over the whole leaded gasoline era (blue) and just between 1925 and 1940 (green; representing source
416 regions outside the Soviet Union). World-wide leaded gasoline emissions were estimated to have peaked
417 in 1970 (Thomas et al., 1997)—an assumption that is supported by the observed timing of the exPb
418 maximum observed in both ice cores. Whilst it is likely that leaded fuel contributed to the increased
419 bromine observed between 1925 and 1970, it is clear that it was not the only contributor to the exBr
420 record, particularly after 1970 when the exBr record continues to rise despite a worldwide decline in
421 leaded fuel consumption. The disparity between the exPb and exBr records suggesting the driving force
422 for the enhanced emission of Br was still active and increasing after 1970.

4.1.3 Seasonal salinity changes

423
424 Younger sea ice surfaces such as frost flowers, new and 1st year sea ice have a higher salinity and thus
425 have higher bromine concentrations than older sea ice surfaces (Hunke et al., 2011) . The salinity of sea
426 ice is at its maximum at the start of the winter season after which surface salinity slowly diminishes due
427 to gravitational draining (Hunke et al., 2011). As summer approaches, ice continues to undergo
428 desalination due to melting of surface snow which percolates through the ice (Hunke et al., 2011).
429 Satellite observations that the BrO flux from the sea ice declines over summer (despite increasing

430   insolation) is likely due to the combined reduction in young sea ice area and in ice salinity. Ocean

431   surface salinity decreases in the summer due to the increased meteoric water flux and melting of

432   desalinated sea ice. Salinity increases are therefore unlikely to be the cause of the exBr flux observed in

433   the ice core records and the observed summer maximum in bromine.

4.1.4 Organic bromine species

435   Gaseous bromocarbons can be a source of inorganic bromine to the snow pack when they react with

436   •OH or to a lesser extent with $\cdot NO_x$ or by photolysis (Kerkweg et al., 2008; WMO, 1995) to form the

437   less reactive, species HBr, $BrNO_3$ and $HOBr$. These species can then be washed out of the atmosphere

438   and deposited on the snow surface due to their high solubility (Fan and Jacob, 1992; Sander et al., 1999;

439   Yung et al., 1980).

440   The predominant source of gaseous bromine in the atmosphere is methyl bromide, CH_3Br (WMO,

441   2002). The major modern sources of CH_3Br are fumigation, biomass burning, leaded fuel combustion,

442   coastal marshes, wetlands, rapeseed and the oceans (WMO, 2002). The ocean is also a major sink for

443   CH_3Br, the temperature sensitive dissolution occurring through hydrolysis and chloride ion substitution

444   to form bromide (WMO, 1995). ~30% of CH_3Br was from industrial emissions at the time of the global

445   peak in the CH_3Br mixing ratio (1996-1998) (Montzka and Reimann, 2010). The timing of the massive

446   increases in inorganic bromine seen at both ice cores sites coincides with the timing of maximum

447   anthropogenic emissions of CH_3Br. However, the estimated 2.7 ppt increase in global tropospheric

448   CH_3Br above preindustrial levels equates to only ~ 3.7 ppt (0.05nM) Br incorporated into the snow

449   pack (assuming 100% conversion efficiency of CH_3Br in soluble Br species). This level is far less than

450   the 2-5 nM increase in exBr observed in the ice cores during the industrial period.

451   Bromoform ($CHBr_3$) is emitted from vegetation such as marine phytoplankton and seaweed. It has the

452   largest globe flux of all the bromocarbons (estimated at almost 5 times that of CH_3Br (Kerkweg et al.,

453   2008). However, it is very short-lived (atmospheric lifetime of ~ 17 days (Ordóñez et al., 2012) and

454   thus is confined to the marine boundary layer. Inorganic bromine formed from the destruction of $CHBr_3$

455   would therefore be representative of only local sources of organic bromine. The biological seasonal

456   cycle maximises the production of $CHBr_3$ in summer and concentrations are greatly reduced but not

457   negligible in winter (tidal forcing also influences bromocarbon emission by allowing coastal algae to

458   dry-out (Kerkweg et al., 2008). The summer maximum in inorganic bromine at Summit (Fig. 3a)

459   suggests that a biogenic source of bromine is dominant. However to-date biogenic sources have been

460   considered insignificant in the Arctic marine boundary layer compared with the inorganic bromine

461   source from sea salts (Simpson et al., 2007). These results suggest that a biogenic system should be

462   reconsidered as a major source of the natural inorganic bromine flux to the polar regions.

463   4.2 Cause of the spring-time increase in bromine flux

464   4.2.1 Bromine explosion events

465   Spring is the time of 'bromine explosion' events above sea ice. Sea salt aerosols passing through these

466   BrO plumes can become enriched with bromine by adsorbing the gaseous species (Fan and Jacob, 1992;

467   Langendörfer et al., 1999; Lehrer et al., 1997; Moldanová and Ljungström, 2001; Sander et al., 2003).

468   Nghiem (2012) showed that these bromine rich air masses can then be elevated above the planetary

469   boundary layer and transported hundreds of kilometres inland. Increasing the frequency and duration of

470   the bromine explosion events would therefore likely increase the amount of bromine delivered to the

471   ice core sites during spring without influencing the total aerosol flux.

472   Spring-time field studies at Ny Ålesund, Svalbard have shown positive correlation between atmospheric

473   filterable bromine species and elevated levels of sulphate and nitrate (Langendörfer et al., 1999; Lehrer

474   et al., 1997) suggesting that acidic, anthropogenic pollution may be the driver of the observed increases

475   in annual bromine enrichment during the industrial period.

476   4.2.2 Acidity effects on debromination

477   In remote, relatively clean environments such as the Arctic, even small increases in acidity are thought

478   to affect the cycling of bromine in the snow pack (Finlayson-Pitts, 2003; Pratt et al., 2013; Sander et al.,

479   1999). In the laboratory, increasing the acidity of frozen (Abbatt et al., 2010) and liquid salt solutions

480   (Frinak and Abbatt, 2006; George and Anastasio, 2007) increased the yield of gas-phase Br_2 whilst at

481   the same increasing the *solubility* of other bromine species, such as HBr. The uptake efficiency of HBr

482   by acidic sulphate aerosols, for example, is estimated at 80% compared to 30% for sea salt aerosols

483   (Parrella et al., 2012). Interestingly, Abbatt (1995) demonstrated that HBr is more than 100 times more

484   soluble in super-cooled sulphuric acid solutions than HCl. This may explain the cause of bromine

485   enrichment in the aerosol measured in the ice cores relative to the more abundant chlorine (Fig. S2).

486   The results of both the laboratory and field studies suggest that increasing snow/ice acidity in the Arctic

487   will likely enhance spring-time bromine explosion events above the sea ice whilst the increase in

488   solubility allows the termination products of the explosion to be transported away from the sites on the

489   surface of acidic aerosols. Increasing spring-time bromine aerosol concentrations would increase the

490   average annual bromine concentrations deposited on the ice sheet and could explain the exBr records

491   observed in both ice cores.

492 Figure 9 illustrates that of the two dominant acidic species preserved in the ice, HNO_3 (represented by

493 nitrate) shows the highest correlation to total bromine over sub-decadal time scales at both ice core sites.

494 Records were detrended with an 11 year running average before comparison to isolate the high

495 frequency components of each record. The bromine – sulfuric acid (represented by sulfate) correlation

496 is not significant. This is primarily because there is no bromine response to the dominant volcanic

497 sulphate spikes throughout the record. The large spikes in sulfate concentrations did not cause a

498 depletion of bromine in the snowpack (Figure 9). This result might be expected if the increased acidity

499 caused more bromine to volatize. These results suggest that HNO_3 is the most influential of the MBL

500 acidic species in the processing and transport of Br on aerosols in the MBL.

4.2.3 NOx and links to bromine

502 The snow and atmospheric chemistries of bromine and nitrate (NO_3^-) are tightly linked. NO_3^- is one of

503 the main sources of the •OH radical. The •OH radical can oxidize bromide salts and cause the release

504 of gas-phase bromine species (Abbatt et al., 2010; Chu and Anastasio, 2005; George and Anastasio,

505 2007; Jacobi et al., 2014). Morin (2008) observed that the majority of nitrate that is deposited to the

506 snow surface is of the form $BrNO_3$ in the coastal Arctic boundary layer. $BrNO_3$ forms by gas-phase

507 reaction of BrO and NO_2. $BrNO_3$ is quickly adsorbed back onto the snow and aerosol surfaces due to

508 its high solubility. The heterogeneous hydrolysis of $BrNO_3$ to again release bromine species back into

509 the gas-phase has also been observed (Parrella et al., 2012) and can occur both during sunlight hours as

510 well as in the dark (Sander et al., 1999). NO_x are intertwined with Br as it cycles between the gas and

511 condensed phases.

512 The seasonality of the NO_3^- signal preserved in the ice cores is coherent with Br, showing a summer-

513 time maximum (Fig. 3a,d). The slight shift in timing of the industrial nitrate seasonal maximum towards

514 spring is replicated in the seasonal bromine signal preserved in the ice (Figure 3). The high correlation

515 between the preindustrial (1750-1850) NO_3^- and Br records (Fig. 9) supports this observation of co-

516 transport and sink of Br and NO_3^- into the snow pack, though the natural sources of each are distinctly

517 different.

518 In the industrial era the low frequency temporal profile of the bromine (Fig. 2) and nitrate records (Fig.

519 4) differ dramatically, apparently questioning the tight relationship observed before 1850. However, the

520 positive correlation between the nitrate and the Br/MSA records is striking at both sites. The large

521 relative increase in bromine (compared with MSA) during the era of high NO_x pollution may point to a

522 non-sea ice source of bromine linked to nitrate emissions.

523 Bromine and NO_x species shared a common source in the 20th century through the combustion of leaded

524   gasoline (Sect. 4.1.2). As discussed above, we observe that leaded fuel pollution reaching the Arctic

525   began to decline after 1970 in-line with reduced global consumption, but the amount of bromine in-

526   excess of natural sources (exBr, Fig. 8) continued to increase – following the trends in NO_x pollution

527   (Fig. 4). The continued increase in NO_x despite the decline in leaded fuel combustion is attributed

528   primarily to biomass burning, soil emissions and unleaded fossil fuel combustion (Lamarque et al.,

529   2013). As the leaded fuel source of bromine began to decline, organic bromine pollutants continued to

530   increase, as was discussed in Sect. 4.1.4. This can only account for a small fraction of the observed Br.

531   The continued correlation between nitrate and exBr despite the decoupling of nitrate and bromine

532   anthropogenic sources after 1970, suggests that nitrate pollution is likely influencing the processing of

533   local, natural sources of bromine in the polar MBL, in effect increasing the mobility of the bromine and

534   thus its flux onto the ice sheet.

4.2.4 Consequences of nitrate driven increased bromine mobility in the Arctic

536   Plumes of BrO emitted from sea ice regions have been linked to mercury deposition events which lead

537   to an increase in the bioavailability of toxic mercury species in polar waters (Parrella et al., 2012).

538   Increased spring-time mobilization of bromine from the sea ice induced by anthropogenic nitrate could

539   therefore increase the frequency and duration of these events and thus the mercury toxicity of the oceans.

540   Increased atmospheric bromine concentrations would also increase the frequency of ozone depletion

541   events (Simpson et al., 2007) thereby altering the oxidative chemistry of the polar MBL.

542   Whilst several studies have begun to explore bromine records from ice cores as a proxy for past sea ice

543   conditions, the results of this study demonstrate that in an era of massive increases in atmospheric acidity

544   the natural relationship between bromine and sea ice conditions can become distorted, precluding it

545   from being an effective modern-day Arctic sea ice proxy.

5   Conclusion

548   In this study we have shown that high resolution MSA measurements preserved in ice cores can be used

549   as a proxy for sea ice conditions (specifically the size of the marginal sea ice zone) along specific

550   sections of the Greenland coast. The MSA records show that sea ice began to decline at the end of the

551   LIA and again, more dramatically during the Industrial period. Also, unsurprisingly, the changes in sea

552   ice conditions in the northern sites have been less dramatic than along the southern coastline.

553   Comparison between the 260 year records of bromine and MSA presented in this study allow us to show

554   that in the preindustrial era bromine concentrations preserved in the Greenland ice sheet are also likely

555   linked to the local sea ice conditions. With the decline of sea ice in the modern era and the dramatic

556   increase in acidic pollutants reaching the Arctic the sea ice-bromine connection is distorted, precluding

557   it from being an effective, direct sea ice proxy during the industrial era. The introduction of NO_x

558   pollution in particular, into the clean Arctic environment promotes mobilization of bromine from the

559   sea ice, which in turn increases the bromine enrichment of the sea salt aerosols, forcing more bromine

560   inland (particularly in spring) than would occur naturally. Whilst Northern Hemisphere pollution may

561   prevent bromine from being an effective modern-day sea ice proxy in the Arctic, in Antarctica the

562   anthropogenic flux of nitrate species is thought to be small in comparison with natural sources (Wolff,

563   2013), leaving room for the possibility that bromine may still be an effective proxy for local Antarctic

564   sea ice conditions.

565

Author contribution

567   Manuscript written and data analysis performed by O.J.M with expert editing by E.S.. Ice cores supplied

568   by J.R.M.. Tunu ice core was collected and processed by O.J.M, J.R.M., N.J.C, M.S., R.H.R. under the

569   leadership of Beth Bergeron. Ice cores dated by M.S., J.R.M.. ICP-MS and CFA measurements

570   performed by O.J.M, J.R.M., N.J.C., L.L, D.P., M.S.. MSA measurements designed and performed by

571   M.G., E.S.

572

Acknowledgements

574   This research was funded by the National Science Foundation; grant numbers 1023672 and 1204176.

575

576 **References**

577 Abbatt, J., Oldridge, N., Symington, a, Chukalovskiy, V., McWhinney, R. D., Sjostedt, S. and Cox, R.

578 a: Release of gas-phase halogens by photolytic generation of OH in frozen halide-nitrate solutions: an

579 active halogen formation mechanism?, J. Phys. Chem. A, 114(23), 6527–33, doi:10.1021/jp102072t,

580 2010.

581 Abbatt, J. P. D.: Interactions of HBr, HCl, and HOBr With Supercooled Sulfuric- Acid-Solutions of

582 Stratospheric Composition, J. Geophys. Res., 100(D7), 14009–14017, 1995.

583 Abbatt, J. P. D., Thomas, J. L., Abrahamsson, K., Boxe, C., Granfors, A., Jones, A. E., King, M. D.,

584 Saiz-Lopez, A., Shepson, P. B., Sodeau, J., Toohey, D. W., Toubin, C., von Glasow, R., Wren, S. N.

585 and Yang, X.: Halogen activation via interactions with environmental ice and snow in the polar lower

586 troposphere and other regions, Atmos. Chem. Phys., 12(14), 6237–6271, doi:10.5194/acp-12-6237-

587 2012, 2012.

588 Abram, N. J., Wolff, E. W. and Curran, M. A. J.: A review of sea ice proxy information from polar ice

589 cores, Quat. Sci. Rev., 79, 168–183, doi:10.1016/j.quascirev.2013.01.011, 2013.

590 Appenzeller, C., Schwander, J., Sommer, S. and Stocker, T. F.: The North Atlantic Oscillation and its

591 imprint on precipitation and ice accumulation in Greenland, Geophys. Res. Lett., 25(11), 1939,

592 doi:10.1029/98GL01227, 1998.

593 Barrie, L. A., Hoff, R. M. and Daggupaty, S. M.: The influence of mid-latitudinal pollution sources on

594 haze in the Canadian arctic, Atmos. Environ., 15(8), 1407–1419, doi:10.1016/0004-6981(81)90347-4,

595 1981.

596 Bertram, F. J. and Kolowich, J. B.: A study of methyl bromide emissions from automobiles burning

597 leaded gasoline using standardized vehicle testing procedures, Geophys. Res. Lett., 27(9), 1423–1426,

598 doi:10.1029/1999GL011008, 2000.

599 Bowen, H. J. M.: Environmental chemistry of the elements / H. J. M. Bowen, Academic Press, London ;

600 New York., 1979.

601 Chen, Q. S., Bromwich, D. H. and Bai, L.: Precipitation over Greenland retrieved by a dynamic method

602 and its relation to cyclonic activity, J. Clim., 10(5), 839–870, 1997.

603 Chu, L. and Anastasio, C.: Formation of hydroxyl radical from the photolysis of frozen hydrogen

604 peroxide, J. Phys. Chem. A, 109(28), 6264–6271, doi:10.1021/jp051415f, 2005.

605 Curran, M. A. J. and Jones, G. B.: Dimethyl sulfide in the Southern Ocean: Seasonality and flux, J.

606 Geophys. Res., 105(D16), 20451, doi:10.1029/2000JD900176, 2000.

507   Curran, M. A. J., van Ommen, T. D., Morgan, V. I., Phillips, K. L. and Palmer, A. S.: Ice core evidence

508   for Antarctic sea ice decline since the 1950s., Science, 302(5648), 1203–1206,

509   doi:10.1126/science.1087888, 2003.

510   Draxler, R. R. and Hess, G. D.: An Overview of the HYSPLIT_4 Modelling System for Trajectories,

511   Dispersion, and Deposition., Aust. Meteorol. Mag., 47(June 1997), 295–308, 1998.

512   Fan, S.-M. and Jacob, D. J.: Surface ozone depletion in Arctic spring sustained by bromine reactions on

513   aerosols, Nature, 359(6395), 522–524, doi:10.1038/359522a0, 1992.

514   Felix, J. D. and Elliott, E. M.: The agricultural history of human-nitrogen interactions as recorded in ice

515   core δ 15 N-NO3−, Geophys. Res. Lett., 40(8), 1642–1646, doi:10.1002/grl.50209, 2013.

516   Finlayson-Pitts, B. J.: The Tropospheric Chemistry of Sea Salt: A Molecular-Level View of the

517   Chemistry of NaCl and NaBr, Chem. Rev., 103(12), 4801–4822, doi:10.1021/cr020653t, 2003.

518   Fischer, H. and Wagenbach, D.: Large-scale spatial trends in recent firn chemistry along an east-west

519   transect through central Greenland, Atmos. Environ., 30(19), 3227–3238, doi:10.1016/1352-

520   2310(96)00092-1, 1996.

521   Frinak, E. K. and Abbatt, J. P. D.: Br2 production from the heterogeneous reaction of gas-phase OH

522   with aqueous salt solutions: Impacts of acidity, halide concentration, and organic surfactants., J. Phys.

523   Chem. A, 110(35), 10456–64, doi:10.1021/jp063165o, 2006.

524   George, I. J. and Anastasio, C.: Release of gaseous bromine from the photolysis of nitrate and hydrogen

525   peroxide in simulated sea-salt solutions, Atmos. Environ., 41(3), 543–553,

526   doi:10.1016/j.atmosenv.2006.08.022, 2007.

527   Hunke, E. C., Notz, D., Turner, A. K. and Vancoppenolle, M.: The multiphase physics of sea ice: a

528   review for model developers, Cryosph., 5(4), 989–1009, doi:10.5194/tc-5-989-2011, 2011.

529   Jacobi, H. W., Kleffmann, J., Villena, G., Wiesen, P., King, M., France, J., Anastasio, C. and Staebler,

530   R.: Role of nitrite in the photochemical formation of radicals in the snow, Environ. Sci. Technol., 48(1),

531   165–172, doi:10.1021/es404002c, 2014.

532   Kahl, J. D. W., Martinez, D. A., Kuhns, H., Davidson, C. I., Jafferezo, J. L. and Harris, J. M.: Air mass

533   trajectories to Summit, Greenland : A 44-year climatology and some episodic events, J. Geophys. Res.

534   Ocean., 102(C12), 26861–26875, 1997.

535   Kerkweg, A., Jöckel, P., Warwick, N., Gebhardt, S., Brenninkmeijer, C. a. M. and Lelieveld, J.:

536   Consistent simulation of bromine chemistry from the marine boundary layer to the stratosphere – Part

537   2 : Bromocarbons, Atmos. Chem. Phys. Discuss., 8(3), 9477–9530, doi:10.5194/acpd-8-9477-2008,

538 2008.

539 Kinnard, C., Zdanowicz, C. M., Koerner, R. M. and Fisher, D. A.: A changing Arctic seasonal ice zone:
540 Observations from 1870-2003 and possible oceanographic consequences, Geophys. Res. Lett., 35(2),
541 2–6, doi:10.1029/2007GL032507, 2008.

542 Lamarque, J.-F., Dentener, F., McConnell, J., Ro, C.-U., Shaw, M., Vet, R., Bergmann, D., Cameron-
543 Smith, P., Dalsoren, S., Doherty, R., Faluvegi, G., Ghan, S. J., Josse, B., Lee, Y. H., MacKenzie, I. A.,
544 Plummer, D., Shindell, D. T., Skeie, R. B., Stevenson, D. S., Strode, S., Zeng, G., Curran, M., Dahl-
545 Jensen, D., Das, S., Fritzsche, D. and Nolan, M.: Multi-model mean nitrogen and sulfur deposition from
546 the Atmospheric Chemistry and Climate Model Intercomparison Project (ACCMIP): evaluation of
547 historical and projected future changes, Atmos. Chem. Phys., 13(16), 7997–8018, doi:10.5194/acp-13-
548 7997-2013, 2013.

549 Langendörfer, U., Lehrer, E., Wagenbach, D. and Platt, U.: Observation of filterable bromine
550 variabilities during Arctic tropospheric ozone depletion events in high (1 hour) time resolution, in
551 Journal of Atmospheric Chemistry, vol. 34, pp. 39–54., 1999.

552 Legrand, M., Hammer, C., De Angelis, M., Savarino, J., Delmas, R., Clausen, H. and Johnsen, S. J.:
553 Sulfur-containing species (methanesulfonate and SO4) over the last climatic cycle in the Greenland Ice
554 Core Project (central Greenland) ice core, J. Geophys. Res., 102(C12), 26663, doi:10.1029/97JC01436,
555 1997.

556 Lehrer, E., Wagenbach, D. and Platt, U.: Aerosol chemical composition during tropospheric ozone
557 depletion at Ny Ålesund/Svalbard, Tellus B, 49(5), doi:10.3402/tellusb.v49i5.15987, 1997.

558 Li, S.-M. and Barrie, L. A.: Biogenic sulfur aerosol in the Arctic troposphere: 1. Contributions to total
559 sulfate, J. Geophys. Res., 98(D11), 20613, doi:10.1029/93JD02234, 1993.

560 Macias Fauria, M., Grinsted, A., Helama, S., Moore, J., Timonen, M., Martma, T., Isaksson, E. and
561 Eronen, M.: Unprecedented low twentieth century winter sea ice extent in the Western Nordic Seas
562 since A.D. 1200, Clim. Dyn., 34(6), 781–795, doi:10.1007/s00382-009-0610-z, 2010.

563 Mann, M. E., Bradley, R. S. and Hughes, M. K.: Global-scale temperature patterns and climate forcing
564 over the past six centuries, Nature, 392(6678), 779–787, doi:10.1038/33859, 1998.

565 McConnell, J. R. and Edwards, R.: Coal burning leaves toxic heavy metal legacy in the Arctic., Proc.
566 Natl. Acad. Sci. U. S. A., 105(34), 12140–12144, doi:10.1073/pnas.0803564105, 2008.

567 McConnell, J. R., Lamorey, G. W., Lambert, S. W. and Taylor, K. C.: Continuous ice-core chemical
568 analyses using inductively coupled plasma mass spectrometry., Environ. Sci. Technol., 36(775), 7–11,

569   doi:10.1021/es011088z, 2002.

570   McConnell, J. R., Edwards, R., Kok, G. L., Flanner, M. G., Zender, C. S., Saltzman, E. S., Banta, J. R.,

571   Pasteris, D. R., Carter, M. M. and Kahl, J. D. W.: 20th-Century Industrial Black Carbon Emissions

572   Altered Arctic Climate Forcing, Science (80-.)., 317(5843), 1381–1384, doi:10.1126/science.1144856,

573   2007.

574   Millero, F. J.: The Physical Chemistry of Seawater, Annu. Rev. Earth Planet. Sci., 2(1), 101–150,

575   doi:10.1146/annurev.ea.02.050174.000533, 1974.

576   Moldanová, J. and Ljungström, E.: Sea-salt aerosol chemistry in coastal areas: A model study, J.

577   Geophys. Res., 106, 1271, doi:10.1029/2000JD900462, 2001.

578   Montzka, S. and Reimann, S.: Scientific Assessment of Ozone Depletion 2010: Scientific Summary

579   Chapter 1 Ozone-Depleting Substances (ODSs) and Related Chemicals. [online] Available from:

580   http://www.esrl.noaa.gov/csd/assessments/ozone/2010/summary/ch1.html (Accessed 23 December

581   2015), 2010.

582   Morin, S., Savarino, J., Frey, M. M., Yan, N., Bekki, S., Bottenheim, J. and Martins, J. M. F.: Tracing

583   the origin and fate of NOx in the Arctic atmosphere using stable isotopes in nitrate., Science, 322(5902),

584   730–2, doi:10.1126/science.1161910, 2008.

585   Mulvaney, R., Pasteur, E. C., Peel, D. A., Saltzman, E. S. and Whung, P.-Y.: The ratio of MSA to non-

586   sea-salt sulphate in Antarctic Peninsula ice cores, Tellus B, 44(4), doi:10.3402/tellusb.v44i4.15457,

587   1992.

588   Nghiem, S. V., Rigor, I. G., Richter, A., Burrows, J. P., Shepson, P. B., Bottenheim, J., Barber, D. G.,

589   Steffen, A., Latonas, J., Wang, F., Stern, G., Clemente-Colón, P., Martin, S., Hall, D. K., Kaleschke, L.,

590   Tackett, P., Neumann, G. and Asplin, M. G.: Field and satellite observations of the formation and

591   distribution of Arctic atmospheric bromine above a rejuvenated sea ice cover, J. Geophys. Res. Atmos.,

592   117(D17), n/a–n/a, doi:10.1029/2011JD016268, 2012.

593   O'Dwyer, J., Isaksson, E., Vinje, T., Jauhiainen, T., Moore, J., Pohjola, V., Vaikmae, R. and van de

594   Wal, R. S. W.: Methanesulfonic acid in a Svalbard ice core as an indicator of ocean climate, Geophys.

595   Res. Lett., 27(8), 1159–1162, doi:10.1029/1999GL011106, 2000.

596   Ordóñez, C., Lamarque, J.-F., Tilmes, S., Kinnison, D. E., Atlas, E. L., Blake, D. R., Sousa Santos, G.,

597   Brasseur, G. and Saiz-Lopez, A.: Bromine and iodine chemistry in a global chemistry-climate model:

598   description and evaluation of very short-lived oceanic sources, Atmos. Chem. Phys., 12(3), 1423–1447,

599   doi:10.5194/acp-12-1423-2012, 2012.

700 Parrella, J. P., Jacob, D. J., Liang, Q., Zhang, Y., Mickley, L. J., Miller, B., Evans, M. J., Yang, X., Pyle,
701 J. A., Theys, N. and Van Roozendael, M.: Tropospheric bromine chemistry: implications for present
702 and pre-industrial ozone and mercury, Atmos. Chem. Phys., 12(15), 6723–6740, doi:10.5194/acp-12-
703 6723-2012, 2012.

704 Pasteris, D. R., McConnell, J. R. and Edwards, R.: High-resolution, continuous method for measurement
705 of acidity in ice cores, Environ. Sci. Technol., 46, 1659–1666, doi:10.1021/es202668n, 2012.

706 Pratt, K. A., Custard, K. D., Shepson, P. B., Douglas, T. A., Pöhler, D., General, S., Zielcke, J., Simpson,
707 W. R., Platt, U., Tanner, D. J., Gregory Huey, L., Carlsen, M. and Stirm, B. H.: Photochemical
708 production of molecular bromine in Arctic surface snowpacks, Nat. Geosci., 6(5), 351–356,
709 doi:10.1038/ngeo1779, 2013.

710 Rankin, A. M., Wolff, E. W. and Martin, S.: Frost flowers: Implications for tropospheric chemistry and
711 ice core interpretation, J. Geophys. Res. Atmos., 107(D23), 4683, doi:10.1029/2002JD002492, 2002.

712 Rayner, N. A.: Global analyses of sea surface temperature, sea ice, and night marine air temperature
713 since the late nineteenth century, J. Geophys. Res., 108(D14), 4407, doi:10.1029/2002JD002670, 2003.

714 Röthlisberger, R., Bigler, M., Hutterli, M., Sommer, S., Stauffer, B., Junghans, H. G. and Wagenbach,
715 D.: Technique for continuous high-resolution analysis of trace substances in firn and ice cores, Environ.
716 Sci. Technol., 34(2), 338–342, doi:10.1021/es9907055, 2000.

717 Röthlisberger, R., Mulvaney, R., Wolff, E. W., Hutterli, M. a., Bigler, M., Sommer, S. and Jouzel, J.:
718 Dust and sea salt variability in central East Antarctica (Dome C) over the last 45 kyrs and its implications
719 for southern high-latitude climate, Geophys. Res. Lett., 29(20), 1–4, doi:10.1029/2003GL016936, 2002.

720 Saltzman, E. S., Dioumaeva, I. and Finley, B. D.: Glacial/interglacial variations in methanesulfonate
721 (MSA) in the Siple Dome ice core, West Antarctica, Geophys. Res. Lett., 33(11), 1–4,
722 doi:10.1029/2005GL025629, 2006.

723 Sander, R., Rudich, Y., von Glasow, R. and Crutzen, P. J.: The role of BrNO3 in marine tropospheric
724 chemistry: A model study, Geophys. Res. Lett., 26(18), 2857–2860, doi:10.1029/1999GL900478, 1999.

725 Sander, R., Keene, W. C., Pszenny, a. a. P., Arimoto, R., Ayers, G. P., Baboukas, E., Cainey, J. M.,
726 Crutzen, P. J., Duce, R. a., Hönninger, G., Huebert, B. J., Maenhaut, W., Mihalopoulos, N., Turekian,
727 V. C. and Van Dingenen, R.: Inorganic bromine in the marine boundary layer: a critical review, Atmos.
728 Chem. Phys. Discuss., 3, 1301–1336, doi:10.5194/acpd-3-2963-2003, 2003.

729 Schönhardt, A., Begoin, M., Richter, A., Wittrock, F., Kaleschke, L., Gómez Martín, J. C. and Burrows,
730 J. P.: Simultaneous satellite observations of IO and BrO over Antarctica, Atmos. Chem. Phys., 12(14),

731   6565–6580, doi:10.5194/acp-12-6565-2012, 2012.

732   Sharma, S., Chan, E., Ishizawa, M., Toom-Sauntry, D., Gong, S. L., Li, S. M., Tarasick, D. W., Leaitch,

733   W. R., Norman, a., Quinn, P. K., Bates, T. S., Levasseur, M., Barrie, L. a. and Maenhaut, W.: Influence

734   of transport and ocean ice extent on biogenic aerosol sulfur in the Arctic atmosphere, J. Geophys. Res.

735   Atmos., 117(12), n/a–n/a, doi:10.1029/2011JD017074, 2012.

736   Sigl, M., McConnell, J. R., Layman, L., Maselli, O. J., McGwire, K., Pasteris, D., Dahl-Jensen, D.,

737   Steffensen, J. P., Vinther, B., Edwards, R., Mulvaney, R. and Kipfstuhl, S.: A new bipolar ice core

738   record of volcanism from WAIS Divide and NEEM and implications for climate forcing of the last 2000

739   years, J. Geophys. Res. Atmos., 118(3), 1151–1169, doi:10.1029/2012JD018603, 2013.

740   Sigl, M., Winstrup, M., McConnell, J. R., Welten, K. C., Plunkett, G., Ludlow, F., Büntgen, U., Caffee,

741   M., Chellman, N., Dahl-Jensen, D., Fischer, H., Kipfstuhl, S., Kostick, C., Maselli, O. J., Mekhaldi, F.,

742   Mulvaney, R., Muscheler, R., Pasteris, D. R., Pilcher, J. R., Salzer, M., Schüpbach, S., Steffensen, J. P.,

743   Vinther, B. M. and Woodruff, T. E.: Timing and climate forcing of volcanic eruptions for the past 2,500

744   years, Nature, 523(7562), 543–9, doi:10.1038/nature14565, 2015.

745   Simpson, W. R., von Glasow, R., Riedel, K., Anderson, P., Ariya, P., Bottenheim, J., Burrows, J.,

746   Carpenter, L. J., Friess, U., Goodsite, M. E., Heard, D., Hutterli, M., Jacobi, H.-W., Kaleschke, L., Neff,

747   B., Plane, J., Platt, U., Richter, a., Roscoe, H., Sander, R., Shepson, P., Sodeau, J., Steffen, a., Wagner,

748   T. and Wolff, E.: Halogens and their role in polar boundary-layer ozone depletion, , 4375–4418,

749   doi:10.5194/acpd-7-4285-2007, 2007.

750   Sjostedt, S. J., Huey, L. G., Tanner, D. J., Peischl, J., Chen, G., Dibb, J. E., Lefer, B., Hutterli, M. a.,

751   Beyersdorf, a. J., Blake, N. J., Blake, D. R., Sueper, D., Ryerson, T., Burkhart, J. and Stohl, a.:

752   Observations of hydroxyl and the sum of peroxy radicals at Summit, Greenland during summer 2003,

753   Atmos. Environ., 41(24), 5122–5137, doi:10.1016/j.atmosenv.2006.06.065, 2007.

754   Smith, S. J., van Aardenne, J., Klimont, Z., Andres, R. J., Volke, A. and Delgado Arias, S.:

755   Anthropogenic sulfur dioxide emissions: 1850–2005, Atmos. Chem. Phys., 11(3), 1101–1116,

756   doi:10.5194/acp-11-1101-2011, 2011.

757   Spolaor, A., Vallelonga, P., Plane, J. M. C., Kehrwald, N., Gabrieli, J., Varin, C., Turetta, C., Cozzi, G.,

758   Kumar, R., Boutron, C. and Barbante, C.: Halogen species record Antarctic sea ice extent over glacial-

759   interglacial periods, Atmos. Chem. Phys., 13, 6623–6635, doi:10.5194/acp-13-6623-2013, 2013a.

760   Spolaor, A., Gabrieli, J., Martma, T., Kohler, J., Björkman, M. B., Isaksson, E., Varin, C., Vallelonga,

761   P., Plane, J. M. C. and Barbante, C.: Sea ice dynamics influence halogen deposition to Svalbard,

762   Cryosph., 7(5), 1645–1658, doi:10.5194/tc-7-1645-2013, 2013b.

763 Spolaor, A., Vallelonga, P., Gabrieli, J., Martma, T., Björkman, M. P., Isaksson, E., Cozzi, G., Turetta,

764 C., Kjær, H. A., Curran, M. A. J., Moy, A. D., Schönhardt, A., Blechschmidt, A.-M., Burrows, J. P.,

765 Plane, J. M. C. and Barbante, C.: Seasonality of halogen deposition in polar snow and ice, Atmos. Chem.

766 Phys., 14(18), 9613–9622, doi:10.5194/acp-14-9613-2014, 2014.

767 Spolaor, A., Opel, T., McConnell, J. R., Maselli, O. J., Spreen, G., Varin, C., Kirchgeorg, T., Fritzsche,

768 D., Saiz-Lopez, A. and Vallelonga, P.: Halogen-based reconstruction of Russian Arctic sea ice area

769 from the Akademii Nauk ice core (Severnaya Zemlya), Cryosph., 10, 245–256, doi:10.5194/tcd-9-4407-

770 2015, 2016.

771 Sturges, W. T. and Harrison, R. M.: Bromine:Lead ratios in airborne particles from urban and rural sites,

772 Atmos. Environ., 20(3), 577–588, doi:10.1016/0004-6981(86)90101-0, 1986.

773 Thomas, V. M., Bedford, J. A. and Cicerone, R. J.: Bromine emissions from leaded gasoline, Geophys.

774 Res. Lett., 24(11), 1371–1374, doi:10.1029/97GL01243, 1997.

775 Vestreng, V., Ntziachristos, L., Semb, A., Reis, S., Isaksen, I. S. A. and Tarrasón, L.: Evolution of NO_x

776 emissions in Europe with focus on road transport control measures, Atmos. Chem. Phys., 9(4), 1503–

777 1520, doi:10.5194/acp-9-1503-2009, 2009.

778 Wagner, T., Leue, C., Wenig, M., Pfeilsticker, K. and Platt, U.: Spatial and temporal distribution of

779 enhanced boundary layer BrO concentrations measured by the GOME instrument aboard ERS-2, J.

780 Geophys. Res., 106(D20), 24225, doi:10.1029/2000JD000201, 2001.

781 Walsh, J. E.: A data set on Northern Hemisphere sea ice extent, Natl. Snow Ice Data Cent., 49–51, 1978.

782 Weißbach, S., Wegner, A., Opel, T., Oerter, H., Vinther, B. M. and Kipfstuhl, S.: Spatial and temporal

783 oxygen isotope variability in northern Greenland - implications for a new climate record over the past

784 millennium, Clim. Past Discuss., 11(3), 2341–2388, doi:10.5194/cpd-11-2341-2015, 2015.

785 Weller, R.: Postdepositional losses of methane sulfonate, nitrate, and chloride at the European Project

786 for Ice Coring in Antarctica deep-drilling site in Dronning Maud Land, Antarctica, J. Geophys. Res.,

787 109(D7), 1–9, doi:10.1029/2003JD004189, 2004.

788 WMO: Scientific Assessment of Ozone Depletion: 1994. Chapter 10: Methyl Bromide, Geneva., 1995.

789 WMO: Scientific Assessment of Ozone Depletion: 2002. Chapter 1: Controlled Substances and Other

790 Source Gases., 2002.

791 Wolff, E. W.: Ice sheets and nitrogen, Philos. Trans. R. Soc. Lond. B. Biol. Sci., 368,

792 doi:10.1098/rstb.2013.0127, 2013.

793 Wolff, E. W., Rankin, A. M. and Röthlisberger, R.: An ice core indicator of Antarctic sea ice

794   production?, Geophys. Res. Lett., 30(22), 2–5, doi:10.1029/2003GL018454, 2003.

795   Xu, L., Russell, L. M., Somerville, R. C. J. and Quinn, P. K.: Frost flower aerosol effects on Arctic

796   wintertime longwave cloud radiative forcing, J. Geophys. Res. Atmos., 118(23), 13282–13291,

797   doi:10.1002/2013JD020554, 2013.

798   Yang, X., Pyle, J. A. and Cox, R. A.: Sea salt aerosol production and bromine release: Role of snow on

799   sea ice, Geophys. Res. Lett., 35(16), 1–5, doi:10.1029/2008GL034536, 2008.

800   Yang, X., Pyle, J. A., Cox, R. A., Theys, N. and Van Roozendael, M.: Snow-sourced bromine and its

801   implications for polar tropospheric ozone, Atmos. Chem. Phys., 10(16), 7763–7773, doi:10.5194/acp-

802   10-7763-2010, 2010.

803   Yung, Y. L., Pinto, J. P., Watson, R. T. and Sander, S. P.: Atmospheric Bromine and Ozone

804   Perturbations in the Lower Stratosphere, J. Atmos. Sci., 37(2), 339–353, doi:10.1175/1520-

805   0469(1980)037<0339:ABAOPI>2.0.CO;2, 1980.

806

807

808

809

310
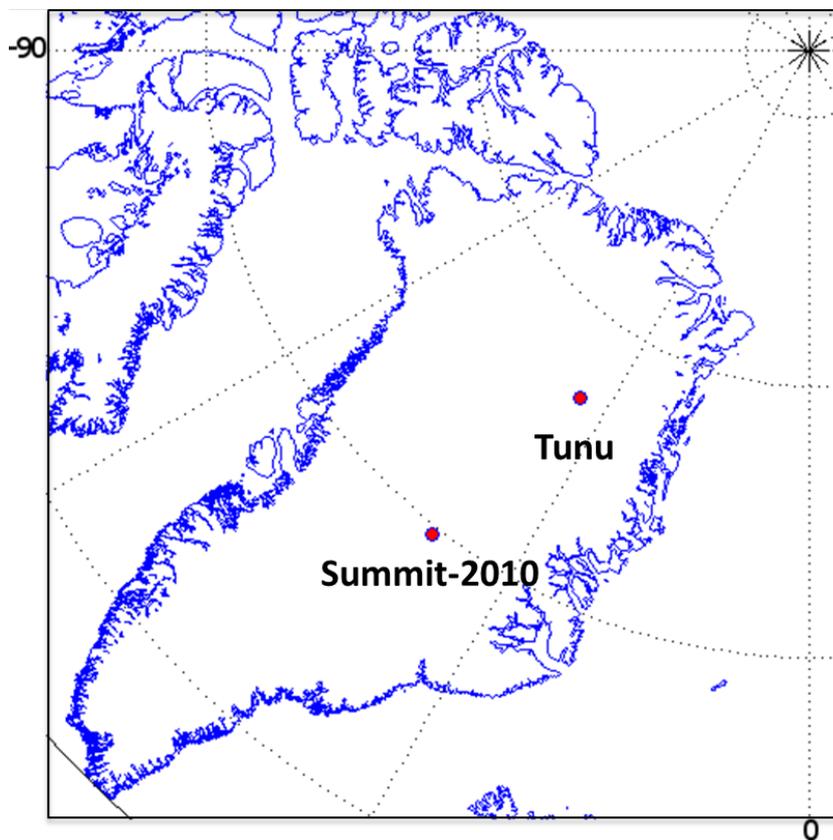
Figure 1. Locations of ice cores used in this study. Summit-2010: (72°20'N 38°17'24"W), Tunu: (78°

2' 5.5"N, 33° 52' 48"W)

311

312

313

314

315

316

317

318

319
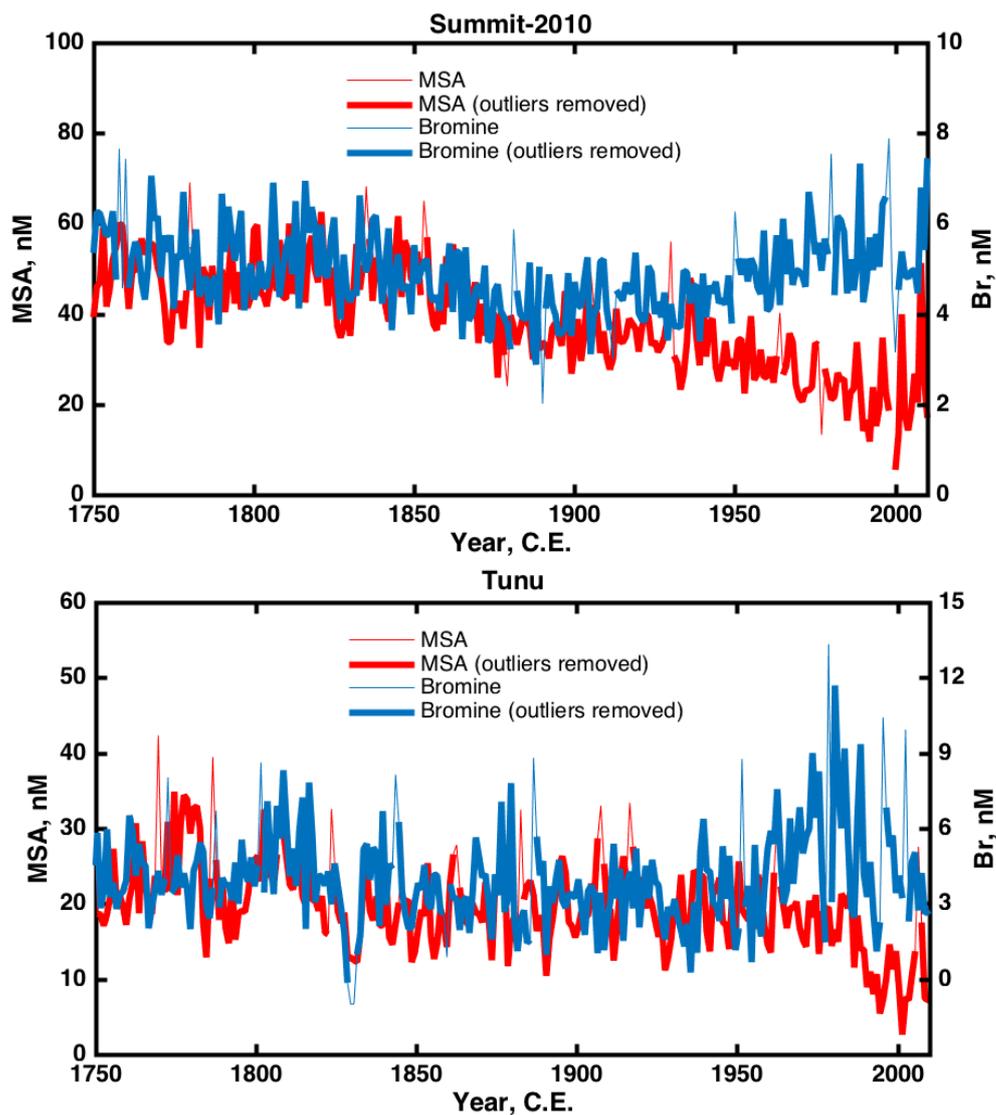
320

321

322   **Figure 2.** Annual record of bromine (thin blue) and MSA (thin red). Annual record of bromine (thick

323   blue) and MSA (thick red) with outlying spikes removed using a 25 year running average filter described

324   by Sigl et al. (2013). All records were fit with a 3 step linear regression and the results of the fits which

325   identify the timing of inflection points are summarized in Table S1.

326
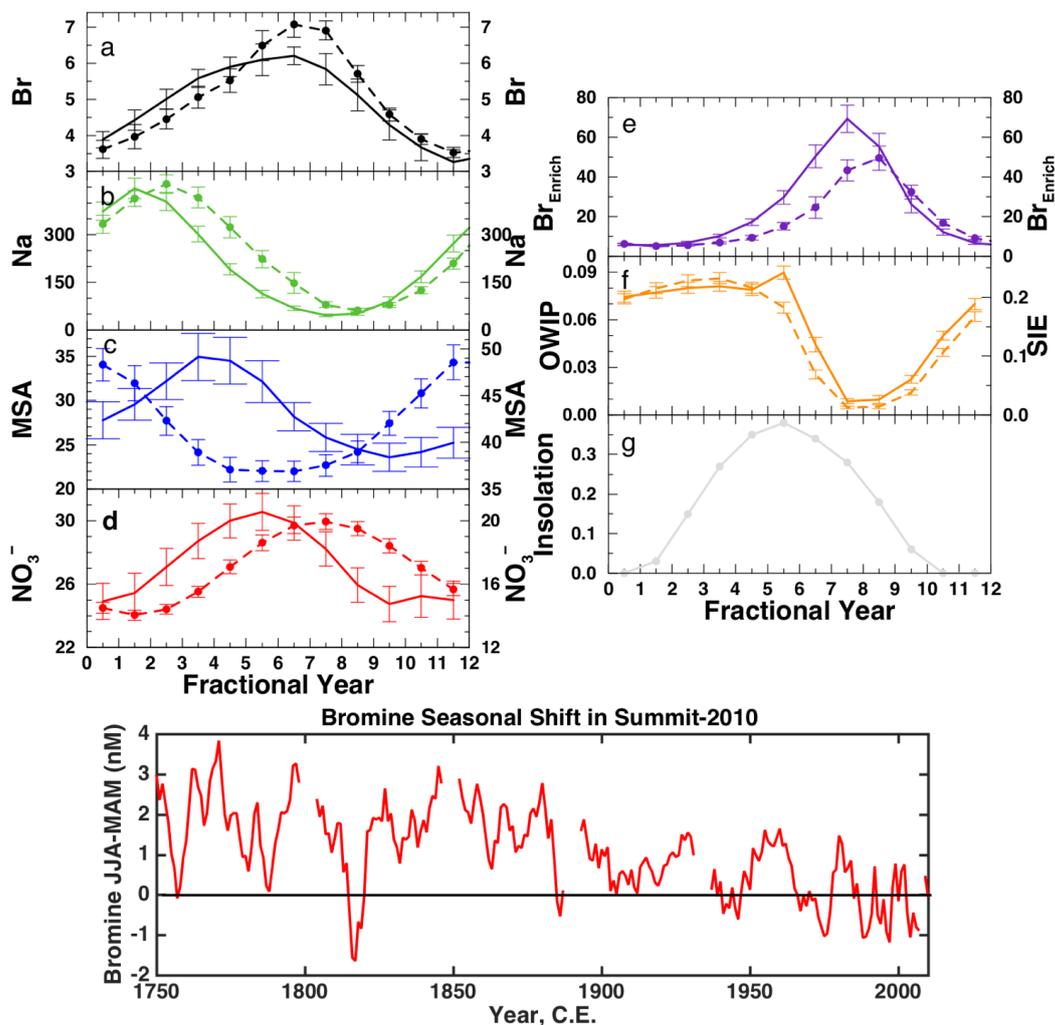
Figure 3. Upper plots: Average seasonal cycle of species in the Summit-2010 ice core. The left-hand Y

axes are associated with the solid lines, and the right-hand Y axes associated with the dashed lines.

Dashed lines (a-e): Average seasonal cycle from depths 43.5 – 87.3 m (years 1742-1900). Solid lines

(a-e): Average seasonal cycle from 0-43.5 m (years 1900-2010). Error bars indicate the standard error

of the monthly value. (a) Total bromine, (b) total sodium, (c) MSA, (d) nitrate. Units for (a-d) are nM.

Note that the seasonal cycle in bromine appears to broaden in the 1900-2010 period (see lower panel).

Note also that the MSA maximum shifts from spring in the shallowest part of the ice core (solid line) to

winter in the deepest part of the ice core (dashed line) due to post-depositional effects (see Fig. S3). (e)

Average seasonal cycle in bromine enrichment (relative to sea salt sodium, see Eq. (4)). (f-right) The

sea ice extent (SIE) within an area of the East Greenland coast [70°− 63° N, 15°− 45° W] that shows

337   highest correlations to MSA (see Fig. 6), (f – left) Area of open water within the sea ice pack (OWIP)

338   for the area defined by SIE. (g) Solar insolation at 12 GMT at the latitude of Summit

339   (eosweb.larc.nasa.gov). Lower plot: Broadening of bromine seasonal cycle in the Summit-2010 ice core.

340   The difference between the summer and spring bromine signal (JJA-MAM) was monitored over the

341   length of the entire ice core. In the preindustrial era (pre-1850) bromine peaks in summer; realised as

342   positive values of JJA-MAM. After 1900 there is a marked broadening of the seasonal signal towards

343   spring and by ~1970 the seasonal signal maximum is routinely shared between summer and spring

344   realised as an averaged JJA-MAM of approximately zero.

345

346
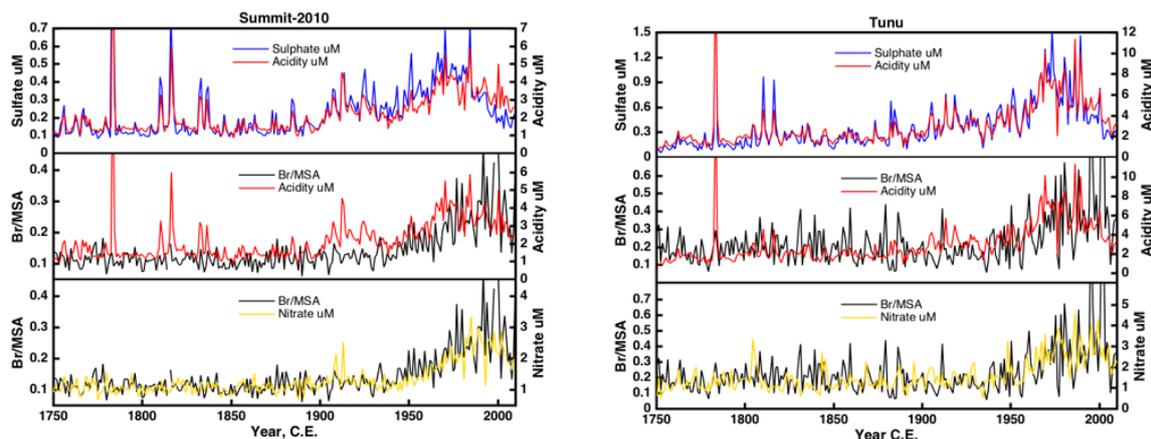
347

348 **Figure 4.** Comparison between the measured total sulfur (shown as sulfate) and acidity records from
349 each ice core (top panels). The acidity record is dominated by the influence of the sulfur species until
350 the early 21th century when the NOx pollution remains elevated whilst anthropogenic sulfur sources are
351 depleted resulting in a slight relative elevation of the total acidity relative to total sulfur concentrations.
352 The large spikes in the acidity and sulfur records are identified as volcanic events. The ice core records
353 cover the period of the 1783 Laki eruption as well as the Unknown 1909 eruption and Tambora eruption
354 (Indonesia) in 1815 (Sigl et al., 2013). Comparison between Br/MSA and total acidity (center panels)
355 and nitrate (NO_3^-, bottom panels) measured in the ice cores. The Br/MSA ratio follows the total acidity
356 record closely except where the record is dominated by the sulphur component (e.g. early 1900s). Of
357 the two major acidic species the Br/MSA follows the nitrate most closely at both ice core sites.

358

359

360

361

362
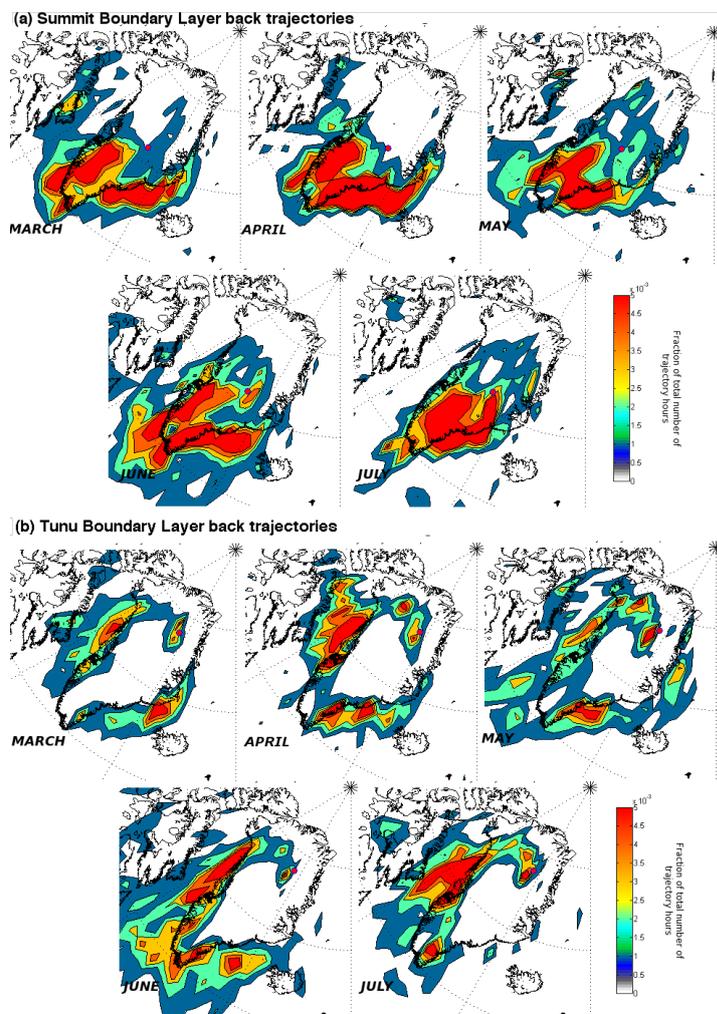
Figure 5. Air mass back trajectories from the (a) Summit-2010 and (b) Tunu ice core sites over the
period 2005-2013 C.E. Maps display the fraction of the total number of trajectory hours (ranging
between 21400-25500 hr month^{-1}) spent at altitudes under 500 m. Back trajectories were allowed to
travel for 10 hr. New trajectories were started every 12 hours. Map grid resolution is 2°x 2°. Ice core
locations are shown by a pink circle. Maps show that air masses consistently arrive at Summit from the
SE Greenland coast with a smaller contribution from the SW coast. Air masses consistently arrive at
Tunu from the western Greenland coast with a smaller contribution from the SE and NE coast. The air
mass originating from the NE coast is most dominant in May and comparison with the total vertical
column profile (Fig. S4) shows it is confined to lower altitudes unlike those from the west coast.

372
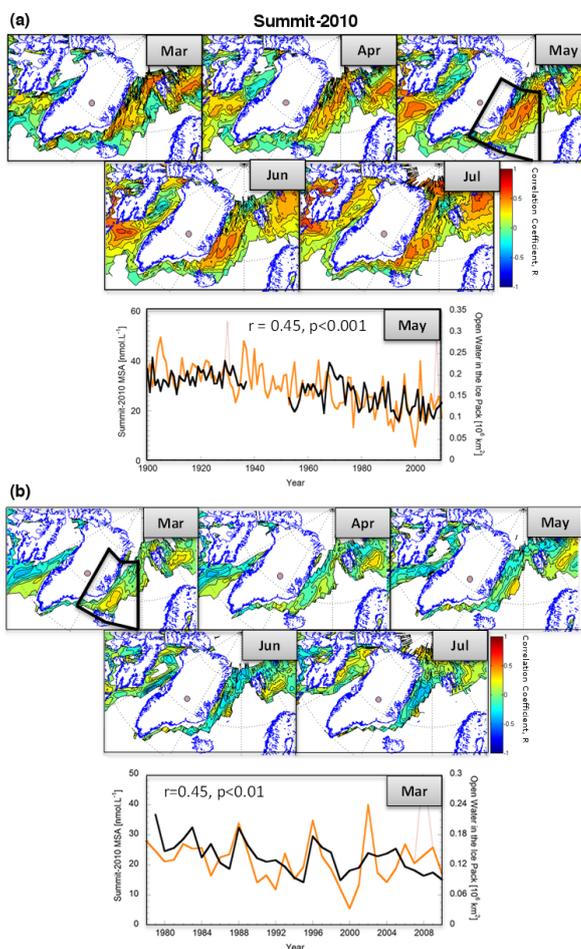
Figure 6. Correlation maps of monthly sea ice concentration (SIC) derived from the Summit-2010 ice
core. (a) HadISST1 ICE dataset from 1900-2012 C.E. correlated with annual records of MSA. Outliers
were removed from the MSA records before the correlations were performed. Month labels indicate
month of SIC compared with the annual MSA value. Only locations that showed a SIC variability
greater than 10% and have a significant correlation (t-test, $p<0.05$) are displayed. The area of sea ice
that is the likely source of MSA (as indicated by the air-mass trajectories) are outlined in black [70°−
63° N, 15°− 45° W]. Graphed is the area of open water in the sea ice in this region (OWIP, black)
overlaid on the annual MSA record (red, outliers removed - orange). (b) As for the upper panel but
focused on the satellite period 1979-2012 C.E. Summit MSA shows a significant, positive correlation
with the amount of OWIP during spring within the integrated region.

383
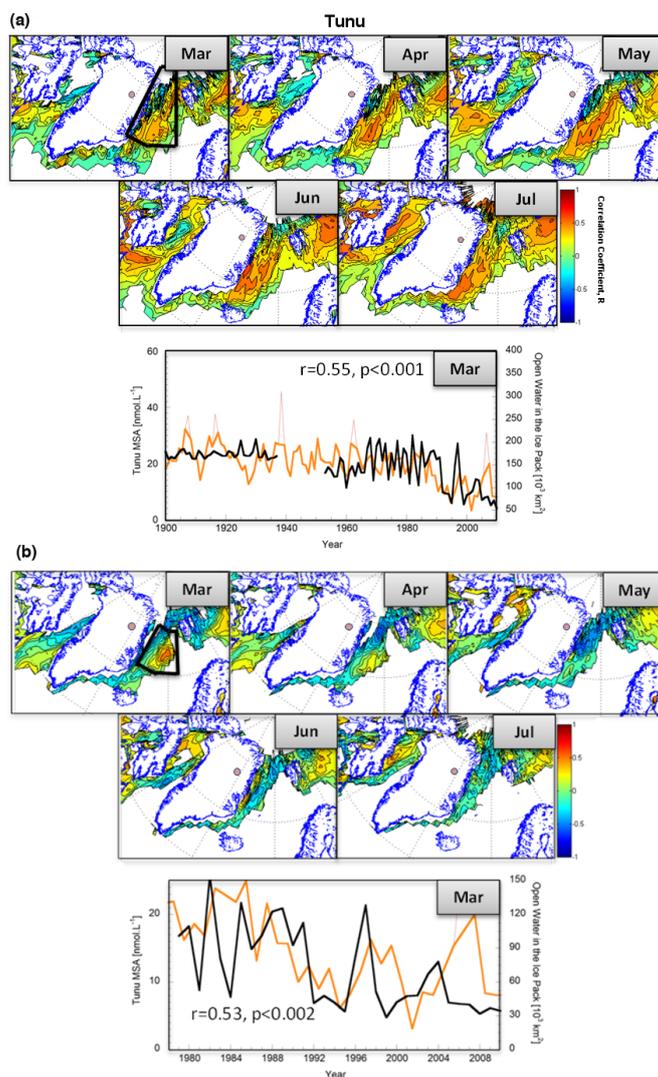
Figure 7. Correlation maps of monthly sea ice concentration (SIC) derived from the Tunu ice core. (a) HadISST1 ICE dataset from 1900-2012 C.E. correlated with annual records of MSA. Outliers were removed from the MSA records before the correlations were performed. Month labels indicate the month of SIC compared with the annual MSA value. Only locations that showed a SIC variability greater than 10% and have a significant correlation (t-test, $p<0.05$) are displayed. The area of sea ice that is the likely source of MSA (as indicated by the air-mass trajectories) are outlined in black [80°− 73° N, 20°− 0° W]. Graphed is the area of open water in the sea ice in this region (OWIP, black) overlaid on the annual MSA record (red, outliers removed - orange). Like in the Summit-20101 ice core, Tunu

MSA also shows a significant, positive correlation with the amount of OWIP during spring but the correlation is highest when MSA is compared to the annual OWIP in the source region. (b) As for the upper panel but focused on the satellite period 1979-2012 C.E. Again MSA shows a significant, positive correlation with the amount of OWIP during spring at both sites. During the satellite period the correlation between OWIP and MSA concentrations at Tunu is greatly increased when a second, closer region is also included in the integration [80°−73° N, 20° −0° W].

899

900
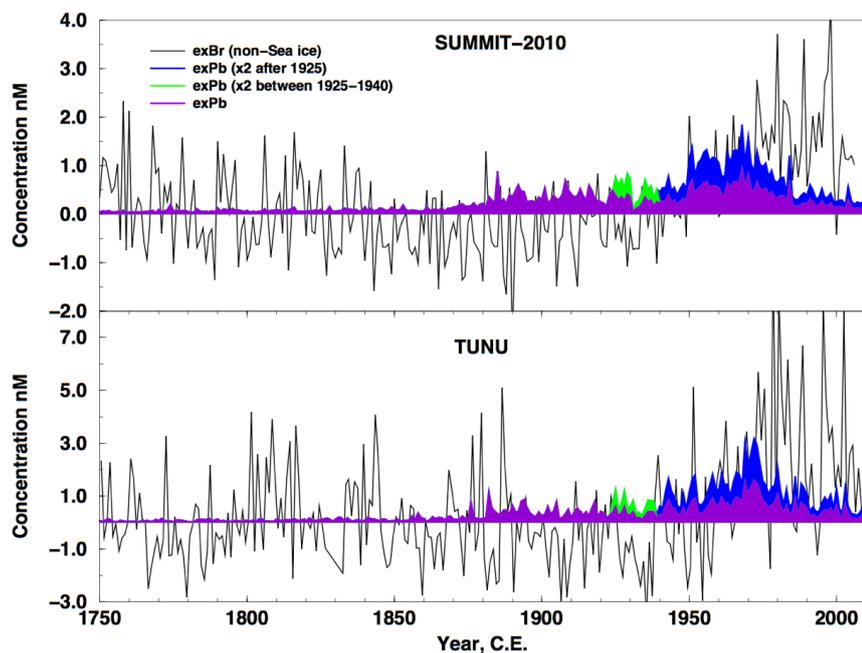
Figure 8. Comparison between measurements of excess lead (exPb, purple shading) and bromine in excess of what is expected from the preindustrial (1750-1880) Br/MSA relationship (exBr, black). Between 1925-1940 world-wide leaded gasoline sources contained a Pb:Br molar ratio of 1:2 (aviation fuel). After 1940 only Russia continued to use the 1:2 ratio in their leaded fuel whilst the rest of the world changed to a 1:1 ratio. The green shading shows an estimate of bromine from leaded fuel combustion over the 1925-1940 period (relative to the exPb concentrations). The blue shading shows the upper limit to the amount of bromine (relative to exPb) that could be derived from leaded fuel combustion by assuming Pb:Br ratio of 1:2 after 1940. After 1970, when world consumption of leaded gasoline began to fall, exBr concentrations continued to rise at both ice core sites far above the concentrations that could be explained by leaded gasoline sources.

911

912

913

914

915
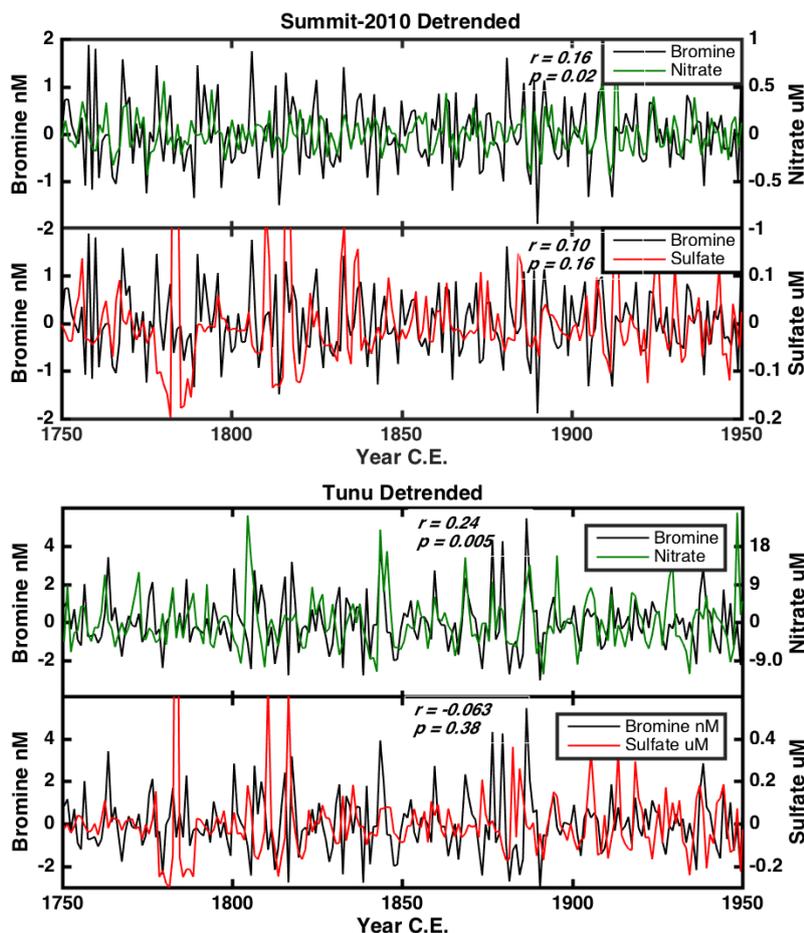
916   **Figure 9.** High frequency comparison between the annual bromine, nitrate and sulfate records measured

917   in the ice cores. Each series has been detrended with an 11 year running average before comparison to

918   remove the low frequency changes in each record. The correlation is highest between bromine and

919   nitrate at both sites. The r-value for bromine versus nitrate at Summit increases in significance (r=

920   0.24,p=0.001) when the entire period (1750-2010) is considered. At both sites there is a close

921   relationship between the variability in the nitrate and bromine due to their intimate relationship during

922   emission from the sea ice, transport and deposition onto the snow pack. The correlation between sulfate

923   (or indeed bulk acidity) and bromine is not significant significant over any of the time periods shown at

924   either site. Particularly evident is the non-response of the bromine signal to the sulfur rich volcanic

925   events as described in Sect.4.2.2.

928